Global Biogeochemical Cycles

RESEARCH ARTICLE
10.1029/2024GB008423

Reconstructing Annual $\Delta^{14}C$ During Miyake Events Using Deciduous and Evergreen Trees

M. R. Walker[1], C. M. Shobe[1,2], L. Andrea-Hayles[3], L. Dey[1], B. Suran[4], B. Nachin[4], and A. E. Hessl[1]

[1]Department of Geology & Geography, West Virginia University, Morgantown, WV, USA, [2]U.S. Forest Service, Rocky Mountain Research Station, Fort Collins, CO, USA, [3]Lamont-Doherty Earth Observatory of Columbia University, Palisades, NY, USA, [4]Department of Environment and Forest Engineering, National University of Mongolia, Ulaanbaatar, Mongolia

Key Points:

- Deciduous and evergreen conifers from the same sites recorded past spikes in atmospheric radiocarbon similarly
- Across multiple sites, modeled radiocarbon production derived from deciduous broadleaf tree results in less certain parameter estimates
- Studies using tree rings to estimate the timing and magnitude of past solar events should consider the physiology of trees

Supporting Information:

Supporting Information may be found in the online version of this article.

Correspondence to:

M. R. Walker,
mrw0044@mix.wvu.edu

Citation:

Walker, M. R., Shobe, C. M., Andrea-Hayles, L., Dey, L., Suran, B., Nachin, B., & Hessl, A. E. (2025). Reconstructing annual $\delta^{14}C$ during Miyake events using deciduous and evergreen trees. *Global Biogeochemical Cycles*, *39*, e2024GB008423. https://doi.org/10.1029/2024GB008423

Received 22 NOV 2024
Accepted 9 JUN 2025

Abstract Cosmic rays and solar energetic particles pose significant risks to satellites, space stations, and human space exploration. They also produce atmospheric radiocarbon (^{14}C), which enters the carbon cycle and is recorded by paleoenvironmental proxies. Miyake events, rapid increases in atmospheric ^{14}C, first identified in annual tree rings and later confirmed through ice core ^{10}Be and ^{36}Cl isotopes, are thought to result from extreme solar activity, are seven events identified over the last 14,300 years. However, uncertainty in annual ^{14}C measurements limits precise inferences about their timing and magnitude. This study examines uncertainties in ^{14}C during two Miyake events (774 CE and 993 CE) across trees with differing uptake, storage, and allocation of carbon. We hypothesize that tree species physiology affects tree-ring $\Delta^{14}C$, with deciduous species recording lagged, attenuated tree-ring $\Delta^{14}C$ relative to evergreen species. Using $\Delta^{14}C$ data from pine and larch in Mongolia and a larger multi-species Northern Hemisphere data set, we employed a Bayesian framework to estimate the timing, duration, and magnitude of these two events. Our AMS results showed no differences in $\Delta^{14}C$ between evergreen and deciduous species growing at similar sites during the 774 CE event. The 993 CE event was variable, but parameter estimates were consistent between species. Northern Hemisphere comparisons indicated that annual series of $\Delta^{14}C$ from evergreen and deciduous conifers yielded relatively more precise modeled estimates of start date and duration relative to deciduous broadleaf species. Future studies should consider the role of species-specific carbon allocation strategies and storage dynamics in determining the radiocarbon response to Miyake events.

1. Introduction

Cosmic rays and solar energetic particles (SEPs) pose significant threats to satellites, space stations, and human space exploration. These particles interact with the Sun's magnetic field, the Earth's geomagnetic field, and the Earth's atmospheric components, resulting in the creation of radioisotopes such as radiocarbon (^{14}C), beryllium-10 (^{10}Be), and chlorine-36 (^{36}Cl), which leave paleo-environmental signatures in tree rings and ice cores. Rapid increases in past atmospheric ^{14}C concentrations, first identified in annual tree ring series (Miyake et al., 2012) and later confirmed as single-year events in ^{10}Be and ^{36}Cl from ice cores (Koldobskiy et al., 2022; Mekhaldi et al., 2015, 2021; Usoskin et al., 2013), provide indirect evidence for studying extreme solar events in the past, essential for evaluating risks associated with severe space-related hazards in our technology-dependent society.

Since the initial discovery of the 774 CE Miyake event, there has been replication of three events: 774 CE (1176 Cal BP), 993 CE (957 Cal BP), and 663 BCE (2610 Cal BP), limited replication of three events: 12,350 BCE (14,300 Cal BP), 7175 BCE (9125 Cal BP), and 5259 BCE (7209 Cal BP), and three proposed extreme ^{14}C production events: 1052 CE (898 Cal BP), 1279 CE (672 Cal BP), and 5411 BCE (7360 Cal BP) (Bard et al., 2023; Brehm et al., 2021, 2022; Miyahara et al., 2022; Miyake et al., 2012, 2013, 2021; Park et al., 2017; Sakurai et al., 2020; Scifo et al., 2024). These ^{14}C production events span 14,300 years and show varying magnitudes based on cosmogenic isotopes in ice cores and tree rings. While estimates of past ^{14}C production vary, some of these past events were ~50 times stronger than the benchmark February 1956 event (Cliver et al., 2022; Golubenko et al., 2025; Rakowski et al., 2022; Usoskin et al., 2013, 2020). The Carrington Event that occurred during September 1859, the strongest solar flare in the observational record, may leave a weak but detectable signal in high latitude conifers relative to those at low latitudes (Uusitalo et al., 2024), supporting the application of ^{14}C in tree rings as a proxy for past solar eruptive events.

Tree-ring reconstructions of past ^{14}C production at the annual time scale rely on uniform carbon uptake and same-season allocation of carbon to wood across tree species and regions. However, ^{14}C in tree rings often shows variability among sites and samples (Miyake et al., 2022; Panyushkina et al., 2024; Uusitalo et al., 2018). This variability might result from a range of factors, including atmospheric mixing (Uusitalo et al., 2024) and species-specific differences in carbon uptake, storage and allocation to wood, which can all influence the incorporation of radiocarbon over time. Variations in leaf phenology and longevity can lead to different periods of carbon gain and may affect the annual course of nonstructural carbohydrates (NSC) in trees (Palacio et al., 2007). Recent studies show that trees store NSCs, such as sugars and starches, which can be repurposed for growth in subsequent seasons (Dietze et al., 2014). These reserves help plants survive under stress and recover from disturbances. The timing and amount of stored versus recently photosynthesized carbon allocated to annual ring growth is uncertain and is likely influenced by factors such as ring anatomy (McDonald et al., 2019), tree stress (Carbone et al., 2013), and species-specific traits (Kagawa et al., 2006; Kudsk et al., 2018). The carbon origin (i.e., stored vs. new) may impact paleosolar studies of ^{14}C that rely on annually to sub-annually resolved tree ring measurements to confirm the timing of past events, identify phase of the 11-year solar cycle, and use latitudinal differences to confirm a solar origin.

Although numerous studies have focused on the timing and magnitude of past Miyake events (Kudsk et al., 2018; Park et al., 2017; Sakurai et al., 2020; Zhang et al., 2022), less attention has been paid to uncertainties related to using $\Delta^{14}C$ from various tree species and sites as a proxy for atmospheric ^{14}C variability on an annual scale. Delta ^{14}C ($\Delta^{14}C$), the ratio of ^{14}C:^{12}C relative to a modern standard, corrected for fractionation and decay, accounts for the tiny fraction of ^{14}C relative to other species of carbon in wood. Several studies have noted the potential effects of different carbon allocation strategies on $\Delta^{14}C$ in annual tree rings (Carbone et al., 2023; Furze et al., 2019; McDonald et al., 2019). One recent study using the 20th century bomb pulse in ^{14}C indicates delays in NSC allocation for a ring porous species (Kromer et al., 2024). However, sample size was limited and the year-to-year change in atmospheric ^{14}C during the 1960s was both larger in magnitude (Hua et al., 2013) and at the same time less abrupt than for Miyake events. The nearly instantaneous nature of Miyake events relative to tree growth combined with the abundance of annual $\Delta^{14}C$ tree ring samples analyzed over these events present a unique opportunity to assess how carbon uptake, storage and allocation in different species influences the reliability of tree rings as an annually resolved proxy for past extremes in ^{14}C production, as well as improving calibration curves for ^{14}C- dating (Heaton et al., 2020).

In this study, we address sources of uncertainty in annual ^{14}C measurements between different tree species using $\Delta^{14}C$ measurements and model-based inferences of start date, duration, phase of the 11-year solar cycle, and ^{14}C excess production of the two best replicated extreme SEP events (774 CE and 993 CE). We hypothesize that tree species physiology affects tree-ring $\Delta^{14}C$ and model-based estimates of past events, with deciduous species recording lagged and attenuated ^{14}C production relative to evergreen species. We contribute new $\Delta^{14}C$ measurements from annual rings of an evergreen conifer (*Pinus sibirica*) and a deciduous conifer (*Larix sibirica*) from similar sites in Mongolia and analyze a larger, multi-species Northern Hemisphere data set that includes deciduous broadleaf species. The primary goal is to advance research on annual $\Delta^{14}C$ measurements in tree rings by examining how carbon uptake and NSC allocation to radial growth might affect modeled inferences about the nature of past Miyake events.

2. Materials and Methods

2.1. Research Sites and Species

Cores and cross sections ($n = 552$) from *Pinus sibirica*, (Siberian pine) and *Larix sibirica*, (Siberian larch) were collected from Khorgo (48.17°, 99.87°) and Uurgat (46.68°, 101.77°) in north-central Mongolia (Figure 1) between 2010 and 2014 (Hessl, Anchukaitis, et al., 2018; Hessl, Pederson, Byambasuren & Nachin, 2018; Hessl, Pederson, Byambasuren, Nachin, & Leland, 2018). *Pinus* and *Larix* species have been widely used for measuring annual values of $\Delta^{14}C$ in tree rings (Büntgen et al., 2018; Jull et al., 2014; Rakowski et al., 2022; Uusitalo et al., 2018). Siberian larch is a deciduous conifer with leaf longevity = 1 year and Siberian pine is an evergreen conifer with leaf longevity estimated at 3–6 years (Schoettle et al., 1994). Leaf longevity affects the timing of carbon uptake and allocation to wood with potential implications for annual records of ^{14}C (Kagawa et al., 2006) with some deciduous trees requiring stored NSCs to initiate growth prior to bud burst (Chen et al., 2022; Hinckley & Lassoie, 1981).

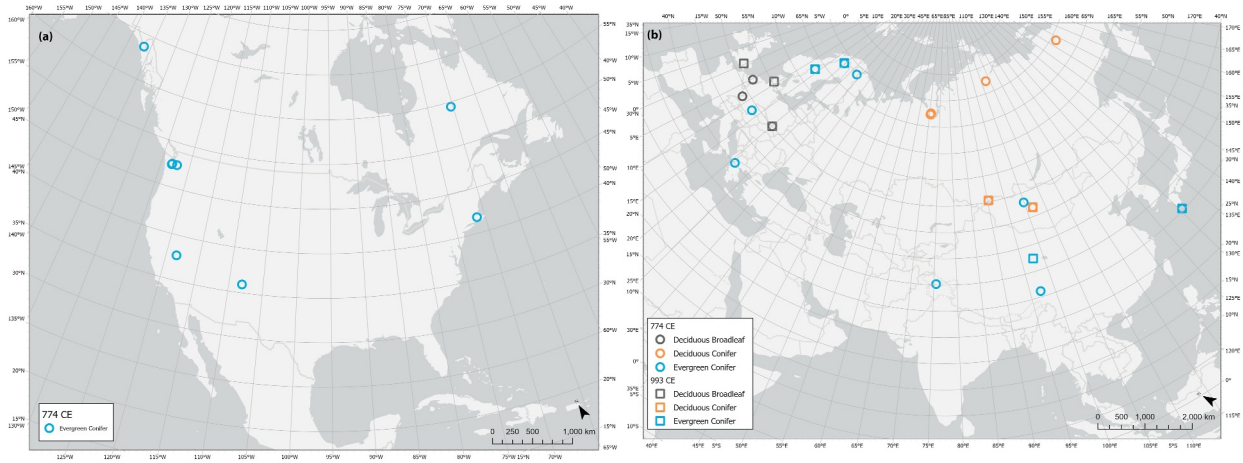

Figure 1. Overview of the Northern Hemisphere tree-ring sites included in this study: (a) sites in North America with blue points representing evergreen conifers; (b) Eurasia with blue points representing evergreen conifers, orange points representing deciduous conifers, and gray points representing deciduous broadleaf.

Samples were collected from living trees growing in thin soils and from dead wood perched on basalt. The sites are continental, within ~300 km of each other and have similar climate and soil conditions (Hessl, Anchukaitis, et al., 2018; Hessl, Pederson, Byambasuren & Nachin, 2018; Hessl, Pederson, Byambasuren, Nachin, & Leland, 2018). The chronologies extend to 668 BCE (Khorgo pine; KLP), 230 CE (Uurgat pine; ULP), 654 BCE (Khorgo larch; KLL) and 416 BCE (Uurgat larch; ULL), with a sample depth of at least 50 samples during 770–780 CE period and at least 62 samples during 990–1000 CE. The average interseries correlations from 700 CE-1000 CE were 0.81 (pine) and 0.69 (larch), indicating that these series are well-dated at annual resolution.

2.2. Sample Selection and Preparation

For each species, we selected cross sections with excellent agreement with the rest of the samples of the chronology (i.e., crossdating) and wide rings oriented parallel to the tangential plane to minimize contamination between rings when sampling (Table S1 in Supporting Information S1). Each cross section was cut into 5 mm thick radial sections, which were then sub sectioned into 3–10 mm thick lathes. We used a flexible microtome blade to hand-section 11 individual rings per lathe centered on the 774 CE and 993 CE events. For the larch cross sections, we separated eight rings into earlywood (EW) and latewood (LW) samples. Pine ring widths were large enough to allow splitting 6 wide rings and homogenizing into two samples (duplicates). Tree-ring samples, weighing approximately 10–60 mg, were stored in polypropylene tubes labeled with the year and tree ID.

To remove mobile compounds and retain only holocellulose, we used a modified base-acid-base-acid-bleaching (BABAB) procedure (Němec et al., 2010; Southon & Magana, 2010). Samples were soaked overnight in 1 ml 1 M NaOH at 75°C and then treated with 1 M HCl and 1 M NaOH for 1 hr each at 75°C. For larger samples, an additional 30-min NaOH treatment was applied. This process removed waxes, fats, oils, and soluble compounds. Next, samples were bleached with 50 ml 1 M HCl and 50 ml 1 M $NaClO_2$ at 75°C for 6 hr, with a second short bleaching required for some samples. After bleaching, the samples were washed with Milli-Q water, dried under a chemical vent hood, and stored in a vacuum desiccator to prevent moisture collection. The final product was pure holocellulose.

2.3. AMS Sample Analysis

Samples were sent to the National Ocean Sciences Accelerator Mass Spectrometry (NOSAMS) laboratory at the Woods Hole Oceanographic Institution for radiocarbon analysis. Pretreated samples were combusted to generate CO_2, which was then reduced into graphite through an automated process. Hydrogen served as the reducing agent to facilitate the carbon reduction. The graphite was compressed into aluminum targets and analyzed using a continuous flow accelerator mass spectrometer, model 1.5SDH-1. Samples were normalized using OX-I and known standards, with blank corrections applied using radiocarbon-free potassium hydrogen phthalate. At NOSAMS, the primary reference material for ^{14}C measurements is NBS Oxalic Acid I (NIST-SRM-4990), which

is used for normalization. Each batch of processed samples includes an appropriate blank and a secondary standard analyzed concurrently for validation.

NOSAMS measures internal statistical error using the total number of ^{14}C counts measured for a target and external statistical error based on the $^{14}C/^{12}C$ of each sample repeated 10 times over the course of a run. The reported error for $\Delta^{14}C$ of each sample is the larger of the two, propagated with errors from normalizing and blank subtraction ("Methods-NOSAMS," 2023; Stuiver & Polach, 1977). All radiocarbon data from NOSAMS are listed in Table S2 in Supporting Information S1.

For the site-level analysis in Mongolia, we also included three $\Delta^{14}C$ series (MON03, MON05 and MON09) from the same sampling locations previously published in Büntgen et al. (2018) (Table S1 in Supporting Information S1). We found no significant difference in mean $\Delta^{14}C$ values between labs (NOSAMS and the ETH Zurich) ($p > 0.05$). Thus, we combined these measurements and errors with those from this study by calculating weighted means and weighted standard errors using inverse-variance weighting for each species and year (Gatz & Smith, 1995; Harrell, 2025; Heckert & Filliben, 2003).

We combined our new $\Delta^{14}C$ measurements with published data from the Northern Hemisphere (Table S2 in Supporting Information S1) and separated the series into evergreen conifers, deciduous conifers (here exclusively larch species), and deciduous broadleaf (here exclusively oak species). We excluded some Büntgen et al. (2018) data noted as "shifted" in the original publication and excluded data from other recent publications where annual variations in ^{14}C were used to date or adjust the dates of samples (Kuitems et al., 2020). Given these criteria, we added five recently published data sets to what was previously analyzed by Zhang et al. (2022) (Black et al., 2023; Pearl et al., 2020; Rakowski et al., 2022). For data sets with repeated measurements or multiple samples within a ring (e.g., earlywood and latewood), we summarized these using a weighted average and weighted AMS error of the $\Delta^{14}C$ values using inverse-variance weighting. With the addition of the eight Mongolian series measured in this study, we compared evergreen conifers ($n = 27$ series, 14 species), deciduous conifers ($n = 13$ series, 3 species) and deciduous broadleaf ($n = 7$ series, 2 species) for the most well-replicated Miyake events: 774 CE (32 total series) and 993 CE (15 total series) (Table S2 in Supporting Information S1). The 663 BCE event, recently dated to 664–663 BCE, shows a non-uniform signal, potentially due to low CO_2 exchange between the trees and surrounding atmosphere as well as prolonged radiocarbon residence in the stratosphere (Panyushkina et al., 2024). Panyushkina et al. (2024) advise against using the event for precise single-year dating. Given these complexities, we excluded it from this study.

2.4. Carbon-Box Modeling

To derive cosmic production rates from raw $\Delta^{14}C$ data, we must model the global carbon cycle, which includes radiocarbon production in the stratosphere and troposphere and its absorption by oceans and the biosphere. Numerous competing models have been developed, each partitioning the Earth system into "boxes" that contain reservoirs of ^{12}C and ^{14}C, along with carbon fluxes between these reservoirs. We combine a carbon-cycle model with Bayesian inference techniques to estimate ^{14}C production rates over time from tree-ring data using the *ticktack* software package (Brehm et al., 2021; Zhang et al., 2022). *ticktack* is a Python framework for reconstructing atmospheric ^{14}C production rates during Miyake events using tree-ring $\Delta^{14}C$ measurements. It estimates ^{14}C production rates by minimizing the misfit between modeled and measured $\Delta^{14}C$ values, thereby yielding best-fit values for the parameters governing ^{14}C production in the model. *ticktack's* SingleFitter class fits the model to a single time series of tree-ring $\Delta^{14}C$ measurements. The MultiFitter class fits multiple ^{14}C time series simultaneously, improving efficiency and capturing variability between different series of annual $\Delta^{14}C$ measurements (Sharma et al., 2023).

Zhang et al. (2022) used SingleFitter to estimate parameters for six Miyake events by dividing them into subsets based on the characteristics of their $\Delta^{14}C$ production rates: those with sharp rises and those with prolonged rises. They then compiled mean $\Delta^{14}C$ time series for each subset to estimate best fit parameters. In contrast, we employed the MultiFitter approach (Sharma et al., 2023) to better capture the variability among series in tree-ring AMS data, which are believed to be over dispersed (Heaton et al., 2020; Scott et al., 2023). We employed the Brehm et al. (2021) 22-box model, simulating the carbon cycle in 11 boxes per hemisphere. For the 774 CE and 993 CE Miyake events, we applied a simple sinusoidal production model with start date, duration, phase of the 11-year solar cycle, and total ^{14}C production as free model parameters. To determine the values for these unknown parameters, we sampled the parameter space and minimized misfit between the model and the data. The

production model describes the production rate $Q(t)$ assuming a steady state mean production rate q_0. This model includes the following components:

$$Q(t) = q_0 + 0.18 * q_0 \sin((2 * \mathrm{pi} * (t + \backslash\varphi)/11\ \mathrm{year})) + S(t, t_0, \Delta t),$$

Where, q_0 represents the baseline production rate prior to the event, φ indicates the phase of the solar cycle, $S(t, t_0, \Delta t)$ denotes the profile of the Miyake event, t_0 is the start time of the event, and Δt is the event duration. Here, t represents time (in years), providing the temporal framework for the production rate and event dynamics. The ^{14}C excess production rate $S(t, t_0, \Delta t, \text{area})$ is modeled by using a super Gaussian of exponent 16. The duration is defined in a way such that the height (or maximum amplitude) of the super Gaussian is equal to area/duration. This model assumes a solar origin; however, since most of the series are 11 years or less, it limits the solar parameters to just the phase of the 11-year solar cycle, with the amplitude of solar modulation fixed at $0.18 * q_0$.

To compare Mongolian pine (evergreen) and larch (deciduous), we modeled each species separately, focusing on how their growth habits affect estimates of past ^{14}C event timing, duration, phase of the 11-year solar cycle, and production. Similarly, at the Northern Hemisphere scale, we used the MultiFitter approach in *ticktack* for each species grouping (evergreen conifers, deciduous conifers, and deciduous broadleaf).

3. Results

3.1. Mongolian Species $\Delta^{14}C$ Comparison

Individual samples of the Mongolian pine and larch $\Delta^{14}C$ maintain similar patterns for the 774 CE event though with greater variation in larch than in pine (Figures 2a and 2b). One pine sample and one larch sample show an early rise in 774 CE (KLP4063 and ULL1006A) with the remainder of samples indicating the initial rise in 775 CE. For all pine and larch samples, the peak values in $\Delta^{14}C$ occur in 775 CE, 776 CE, and/or 777 CE after which $\Delta^{14}C$ declines. Mean annual values of $\Delta^{14}C$ for pine and larch record similar timing, peak in $\Delta^{14}C$, and overall pattern of the event (Figure 3a). In the mean series, the greatest rise in $\Delta^{14}C$ occurs between 774 and 775 CE for pine (12.07‰, SE = 2.79‰) and for larch (12.00‰, SE = 2.92‰), where SE includes propagated uncertainty among the two years of measurements.

For the 993 CE event, individual samples of $\Delta^{14}C$ from pine and larch are more variable than for the 774 CE event, with larch showing the greatest variation (Figures 2c and 2d). Mean annual values of $\Delta^{14}C$ for both pine and larch show a less abrupt rise in $\Delta^{14}C$ compared to the 774 CE event (Figures 3a and 3b), with larch showing a rise beginning in 992 CE and in pine showing no significant departure until 994 CE. In pine, $\Delta^{14}C$ values remain enriched through 999 CE, whereas in larch, they decline after 996 CE. The overall rise in pine from 992 to 999 CE is 7.16‰ (SE = 2.41‰ where SE includes propagated uncertainty among 992 and 999 values), while in larch the rise from 992 to 996 CE is 10.16‰ (SE = 2.33‰, where SE includes propagated uncertainty among 992 and 996 values).

3.2. Modeling ^{14}C Production Using Two Mongolian Conifers

We used *ticktack* to evaluate whether differences in the physiology of two Mongolian conifers affect estimates of the timing, duration, and ^{14}C production of Miyake events inferred from fitting a carbon cycle box model to tree-ring $\Delta^{14}C$ measurements. Posterior parameter distributions represent the probability distributions of parameter values, where the peaks (modal values) indicate the values with the highest likelihood of being true given the $\Delta^{14}C$ measurement series.

The posterior parameter distributions (Figures 4a–4d) and modal values (Table S4 in Supporting Information S1) for pine and larch during the 774 CE event are remarkably similar between species for start date (modes for pine = 774.53 CE, 95% CI of [773.71, 774.96] and larch = 774.55 CE, 95% CI of [774.05, 774.77]), duration (modes for pine = 0.09 year, 95% CI of [0.04, 1.73]; larch = 0.08 year, 95% CI of [0.04, 1.28]), and production (modes for pine = 6.02 atoms/cm^2 year/s, 95% CI of [5.49, 6.68]; larch = 6.21 atoms/cm^2 year/s, 95% CI of [5.78, 6.62]). Modal values for phase of the 11-year solar cycle are also similar (pine = −0.65 φ year, 95% CI of [−3.06, 2.15]; larch = 1.11 φ year, 95% CI of [0.11, 2.25), though the distribution is wider for pine compared to larch. There is a consistent negative correlation between estimated parameter values for start date and duration across all models runs for each species (Figures S1 through S10 in Supporting Information S1).

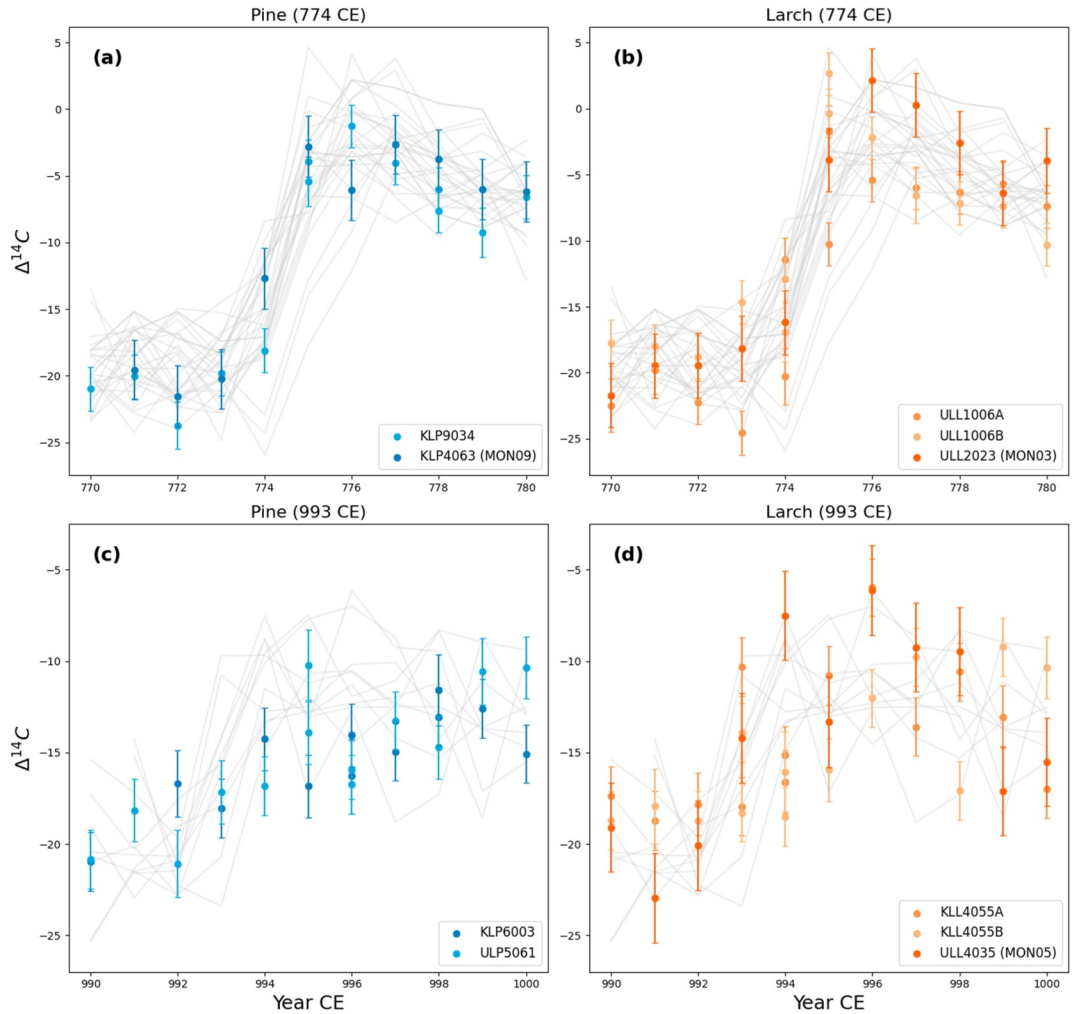

Figure 2. Annual $\Delta^{14}C$ measurements of Siberian pine and Siberian larch during the 774 CE (a, b) and 993 CE (c, d) events, with error bars representing the instrumental error in $\Delta^{14}C$ for each sample as reported by National Ocean Sciences Accelerator Mass Spectrometry and the ETH Zurich. Gray lines are previously published $\Delta^{14}C$ values from Northern Hemisphere sites (Black et al., 2023; Brehm et al., 2022; Büntgen et al., 2018; Fogtmann-Schulz et al., 2017; Jull et al., 2014; Miyake et al., 2012, 2013; Pearl et al., 2020; Rakowski et al., 2015, 2018, 2022; Scifo et al., 2019; Uusitalo et al., 2018).

Posterior parameter distributions for the 993 CE event generally have wider distributions compared to those of 774 CE, consistent with the large variation in the measured $\Delta^{14}C$ data and the slow rise in measured $\Delta^{14}C$ values (Figures 4e–4h, Table S5 in Supporting Information S1). This is especially true of pine, where the density plots for start date, duration and production are broad (Figures 4e–4h). Modal values for phase of the 11-year solar cycle are similar between the two species (pine = 0.32 φ year, 95% CIs of [−2.36, 1.87]; larch = 0.38 φ year, 95% CIs of [0.05, 1.60]), as are production (pine = 2.94 atoms/cm^2 year/s, 95% CIs of [2.06, 16.38]; larch = 2.56 atoms/cm^2 year/s, 95% CIs [2.10, 2.93]), though the distribution of the posterior estimate of the ^{14}C-excess production in larch is considerably narrower.

3.3. Northern Hemisphere Modeling

Using methods similar to those applied for Mongolian larch and pine, we used *ticktack* to evaluate whether differences in the physiology of evergreen conifer, deciduous conifer and deciduous broadleaf species from a larger Northern Hemisphere data set affect modeled estimates of the timing, duration, and ^{14}C excess production of Miyake events. Before the Miyake event, the estimated $\Delta^{14}C$ baseline for years (770–773 CE, 990–992 CE) showed good agreement with the raw $\Delta^{14}C$ data across species groups, noting that there were only three series of deciduous broadleaf trees for the 774 CE event (Figures S11 through S12 in Supporting Information S1). Modeled

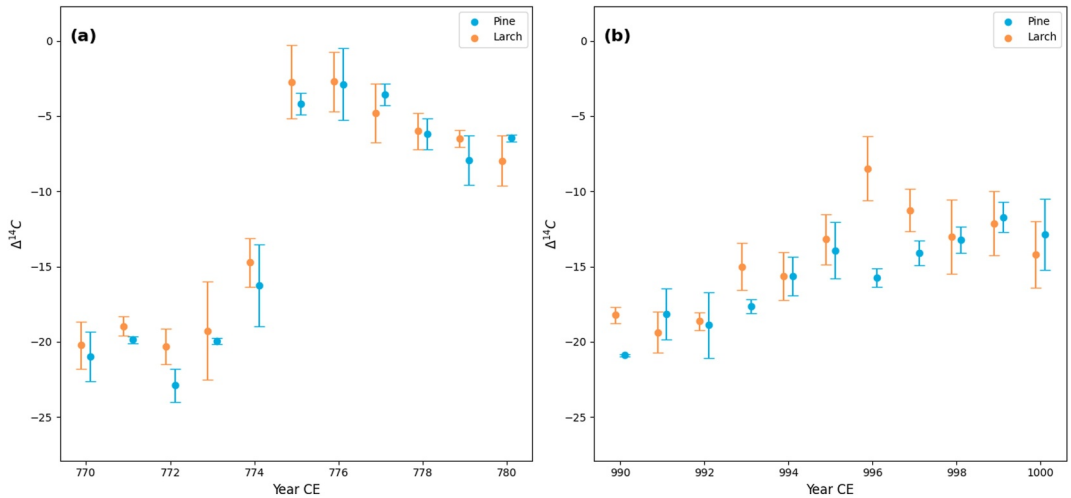

Figure 3. Weighted mean (circles) and weighted standard error (bars) of $\Delta^{14}C$ from annual measurements of Siberian pine (blue) and Siberian larch (orange) during 774 CE event (a) and the 993 CE event (b). Note that where replicate values cluster tightly, the propagated error diminishes accordingly. Thus, for pine in 771, 773, and 780, and 990 CE, the sample AMS measurements and their errors were similar (see Figure 2a), resulting in propagated error that is less than instrument error. The instrumental error reported by National Ocean Sciences Accelerator Mass Spectrometry is plotted for the single pine measurements in 770 CE (KLP9034 ± 1.65‰) and 991 CE (KLP5091; ±1.36‰).

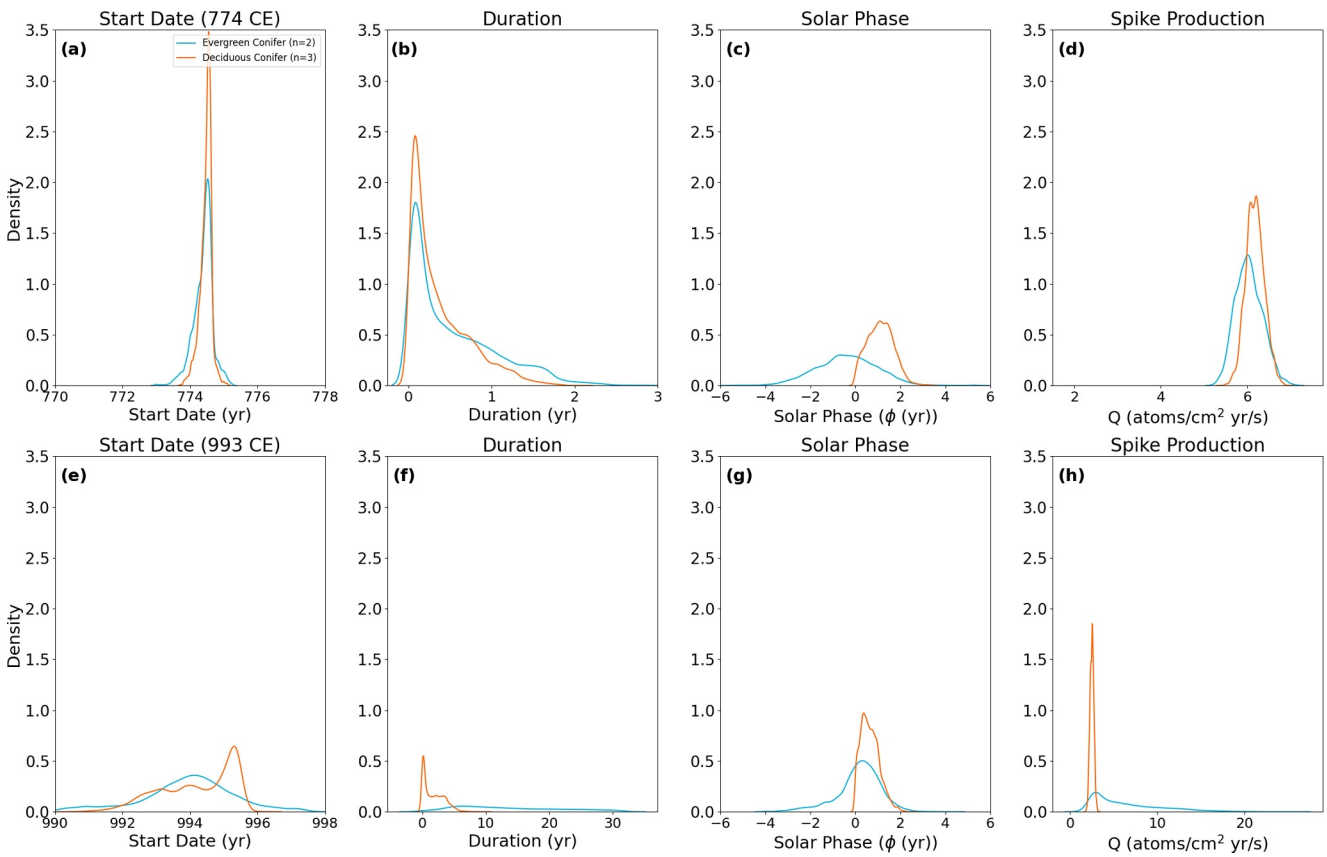

Figure 4. Kernel density plots of posterior distributions for start date, duration, phase of the 11-year solar cycle, and ^{14}C excess production from Mongolian Siberian pine ($n = 2$) and Siberian larch ($n = 3$) $\Delta^{14}C$ data sets for the (a–d) 774 CE event and (e–h) 993 CE event.

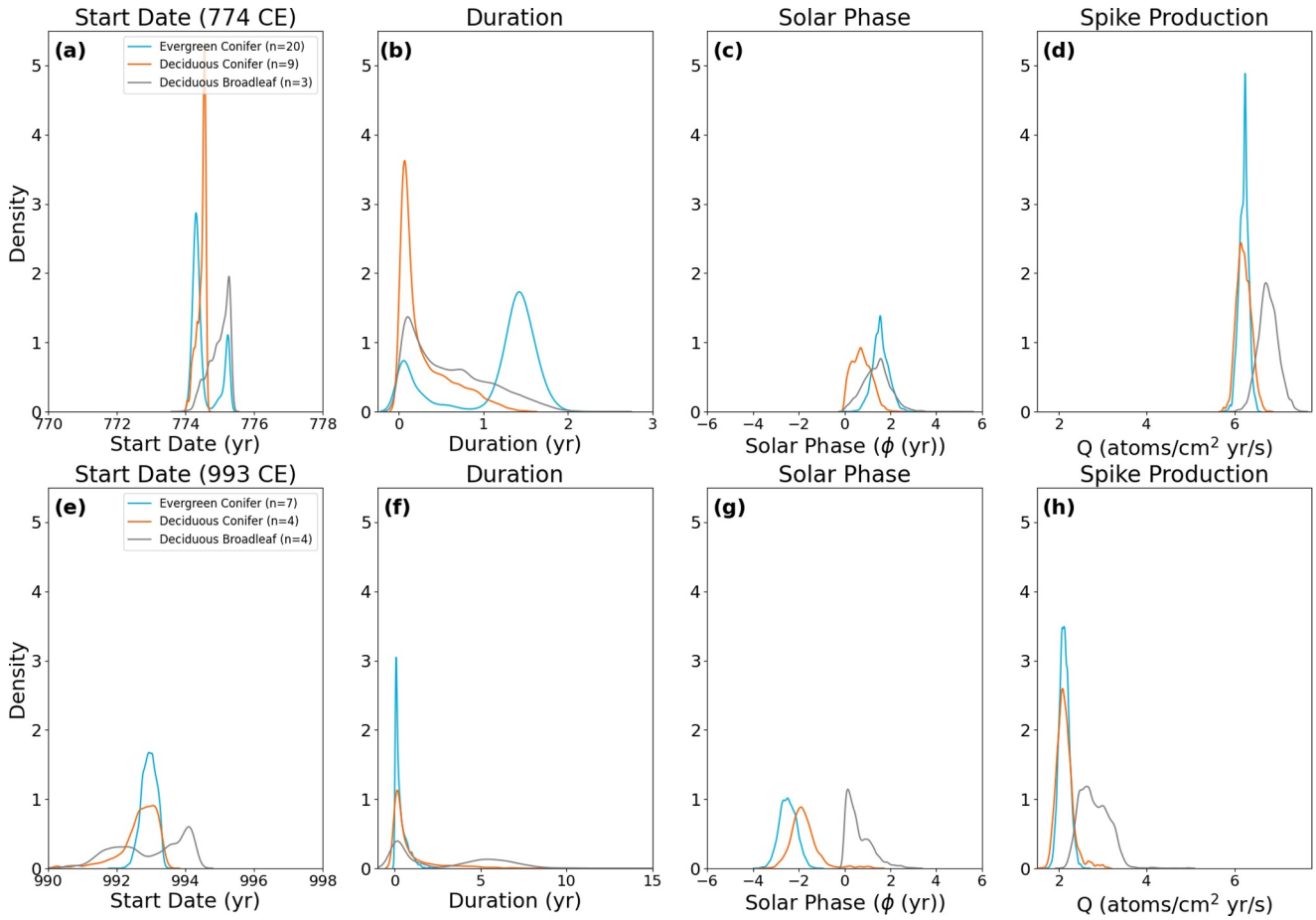

Figure 5. Kernel density plot of posterior distributions for start date, duration, phase of the 11-year solar cycle, and ^{14}C excess production from Northern Hemisphere Δ^{14}C (Black et al., 2023; Brehm et al., 2022; Büntgen et al., 2018; Fogtmann-Schulz et al., 2017; Jull et al., 2014; Miyake et al., 2012, 2013; Pearl et al., 2020; Rakowski et al., 2015, 2018, 2022; Scifo et al., 2019; Uusitalo et al., 2018) and Mongolian Siberian pine and larch Δ^{14}C data set comparing evergreen conifer (n = 27), deciduous conifer (n = 13) and deciduous broadleaf (n = 7) data sets for the (a–d) 774/775 CE event, (e–h) 993/994 CE event.

Δ^{14}C time series also captured the observed timing of the initial rise in measured Δ^{14}C among evergreen conifers, with a gradual rise beginning in 774 CE and continuing to 776 CE (Figure S11a in Supporting Information S1). For deciduous conifers, the modeled increase in tree ring Δ^{14}C starts later with an abrupt rise placed at ~775 CE (Figure S11c in Supporting Information S1). In contrast, measured Δ^{14}C in broadleaf deciduous trees document a rise in 775 CE, with a peak in 776 CE, but the model indicates an abrupt rise at ~775.3 CE, likely due to the elevated values in 776 and 777 CE.

These patterns in the timing of the modeled Δ^{14}C time series are reflected in the posterior distributions for the start date. In the case of 774 CE, the model produces a distribution of start date for deciduous broadleaf that is much broader than the other groups and, though the distribution for start date overlaps with uncertainty of the other groups, modal start is delayed by approximately 1 year (evergreen conifer = 774.3, 95% CI of [774.14, 775.27], deciduous conifer = 774.6, 95% CI of [774.15, 774.62] deciduous broadleaf = 775.3, 95% CI of [774.32, 775.34]) (Figure 5a, Table S4 in Supporting Information S1). A subset of evergreen conifers also produces a secondary and later modeled peak in the start date that affects the shape of the distribution for this group. Five series contribute to this secondary peak: three series from coastal Washington (Black et al., 2023), one series from Sweden (Büntgen et al., 2018) and one series from coastal Japan (Büntgen et al., 2018), each with modal start dates of ~775 CE or ~776 CE (Figure S13 in Supporting Information S1). For the 993 CE event, evergreen and deciduous conifers produce similar modal values for the start date (Figure 5e, Table S5 in Supporting Information S1), though these are broader and less certain than for the 774 CE event. The distribution of parameter estimates for start date among the deciduous broadleaf is broad and bimodal, with a lower peak in ~992 CE and a higher peak in ~994 CE.

Again, modal values are ~1 year later than for the other two species groups, though all distributions overlap within the 95% confidence intervals (Table S5 in Supporting Information S1).

For most species groups and both events, the distributions of event duration are centered close to 0 with long tails skewed toward longer durations (Figures 5b and 5f, Tables S4 and S5 in Supporting Information S1). For the evergreen conifer in 774 CE and for deciduous broadleaf groups in 993 CE, the distribution of duration estimates is bimodal and in both cases, this reflects the bimodal distribution of modeled start date. The distributions of the posterior estimate of the 11-year solar cycle phase are broadly comparable among the species groups for both events (Figures 5c and 5g). Model estimates suggest that the 774 CE event occurred shortly after a solar minimum (modal values for 774 CE evergreen conifer = 1.56φ year, 95% CIs of [0.88, 2.30], 774 CE deciduous conifer = 0.70φ year, 95% CIs of [0.06, 1.56], and 774 CE deciduous broadleaf = 1.58φ year, 95% CIs of [0.26, 2.57]), while model estimates indicate the 993 CE event occurred right before or during a solar minimum (modal values for 993 CE evergreen conifer = -2.49φ year, 95% CIs of [−3.18, −1.74] 993 CE deciduous conifer = -1.91φ year, 95% CIs of [−2.75, 0.17] and 993 CE deciduous broadleaf = 0.14φ year, 95% CIs of [0.01, 2.06]) (Figure 5g).

Modal values for ^{14}C excess production for the 774 CE event are similar across all groups (evergreen conifer = 6.24 atoms/cm^2 year/s, 95% CIs of [5.99, 6.41] deciduous conifer = 6.14 atoms/cm^2 year/s, 95% CIs of [5.93, 6.53]; deciduous broadleaf = 6.71 atoms/cm^2 year/s, 95% CIs of [6.34, 7.21]) with all parameter values falling within uncertainty (Figure 5d and Table S5 in Supporting Information S1). However, the distribution for the broadleaf deciduous group is broader, reflecting less certainty relative to the other species groups. For the 993 CE event, modal estimates of production are also similar among all three groups (evergreen conifer = 2.12 atoms/cm^2 year/s, 95% CIs of [1.91, 2.36]; deciduous conifer = 2.08 atoms/cm^2 year/s, 95% CIs of [1.83, 2.65]; and deciduous broadleaf = 2.64 atoms/cm^2 year/s, 95% CIs of [2.30, 3.42]) (Figure 5h) Again, the conifer groups produce narrower distributions of production compared to the deciduous broadleaf group which produced a highly skewed distribution with the tail extending to ~5 atoms/cm year/s.

4. Discussion

Our study demonstrates that the evergreen and deciduous conifers growing at similar sites exhibit similar patterns of radiocarbon uptake and allocation to wood during Miyake events. Since some evidence indicates that early-wood formation in deciduous conifers occurs around the time of budburst (Barbaroux & Bréda, 2002; Epron et al., 2012; Hinckley & Lassoie, 1981), we expected to observe a delay in the timing of Miyake events as recorded by deciduous conifers. Instead, our study of two species from similar sites demonstrates surprising synchronicity, especially for the 774 CE event, likely a result of the shared wood anatomy and carbon allocation strategies among conifers (Chen et al., 2022; Hinckley & Lassoie, 1981). In European larch, needles emerge just 2–3 weeks prior to stem growth (Moser et al., 2010; Rossi et al., 2009), suggesting that the timing of uptake and allocation to wood may be more closely aligned than previously thought. However, recent studies of NSCs in conifers suggest that "old" stored carbon compounds generated in previous growing seasons contribute to new wood formation (Epron et al., 2012; Peltier et al., 2023; Von Felten et al., 2007), particularly when trees are under stress. Because the Siberian larch and Siberian pine sampled here were growing under similarly stressful conditions (Hessl, Anchukaitis, et al., 2018; Hessl, Pederson, Byambasuren & Nachin, 2018; Hessl, Pederson, Byambasuren, Nachin, & Leland, 2018), these effects would not be distinguishable between the two species. However, one larch and one pine series show an early start for the 774 CE event relative to other series from the same sites, suggesting that variability between individual trees may impact the results. Additional studies on how old NSCs contribute to cellulose in the wood of stressed trees, typical of long tree ring records, are needed. Nevertheless, the modeled timing, duration, and inferred ^{14}C excess production of the 774 CE Miyake event is similar to previously published findings for Northern Hemisphere mid- to high- latitude conifers (Büntgen et al., 2018), supporting overall same-year uptake and allocation to wood among the two conifer species we sampled.

At the Northern Hemisphere scale, we also observed relatively similar modeled responses in timing, duration, and excess ^{14}C production during Miyake events across evergreen conifer, deciduous conifer, and broadleaf deciduous groups, though additional variation arising from latitude, elevation, local atmospheric circulation and other regional offsets likely contributed to variation in parameter distributions (Miyake et al., 2022; Reimer et al., 2020; Uusitalo et al., 2018). Similar to the results of Zhang et al. (2022), we found a subset of trees that result in a

delayed rise (start date) in modeled ^{14}C production for the 774 CE event. We observe that a small subset of evergreen conifers created secondary peaks in modeled start dates and consequently variable event durations. The coniferous series from Sweden, along with those from coastal locations in Washington and Japan (Black et al., 2023; Büntgen et al., 2018), had a delayed rise and modeled start date for the 774 CE event (Figure S13 in Supporting Information S1). Both Japan and western Washington are located near regions of upwelling of old, ^{14}C-depleted water. Variable coastal winds carrying this depleted CO_2 could impact radiocarbon signals by mixing this old carbon with that produced during the Miyake event (Appenzeller et al., 1996; Braziunas et al., 1995; Nakamura et al., 2013). The outlier observed in the Sweden series could result from a range of factors, including altitude, soil respiration, or wind speeds (Reimer et al., 2020; Rodgers et al., 2011; Schuur & Trumbore, 2006). The evergreen conifers included in this study span a wide range of latitudes (30.33°–68.50°), species, and environmental conditions. In contrast, the deciduous conifer group, comprising a single genus (larch) from a narrower range of high latitudes (46.67°N–72.22°N), yield more precise parameter estimates. The variations observed here point to site-specific conditions that likely complicate the detection of uniform event signals across different geographic locations, especially when single sites with limited samples are used for reconstructing paleo-solar events.

Compared to conifers, the deciduous broadleaf series, here made up of ring-porous oaks, produces more variable modeled responses to both Miyake events, noting that there is less replication for this group. While the posterior parameter distributions for deciduous broadleaf series overlapped with the 95% CIs of the conifers, the oak series resulted in wider posterior distributions and therefore reduced model precision for some parameters. Among the conifer groups, the deciduous conifers (here larch species exclusively) produced narrower posterior distributions in most cases, though results were similar to the much larger evergreen conifer group. We argue that these differences in parameter distributions are due to how different tree types make use of non-structural carbohydrates in wood formation. Unlike conifers, ring-porous species rely heavily on the storage of NSCs since they must draw upon these reserves to initiate water transport prior to bud break (Barbaroux & Bréda, 2002; Epron et al., 2012; Hinckley & Lassoie, 1981). Deciduous broadleaf species have higher total NSC concentrations than evergreen conifer species, and in comparisons between species, some of the highest NSCs in wood have been observed in oak (Richardson et al., 2013). In one study, oaks stored nearly four times the amount of NSCs in wood compared with pine (Richardson et al., 2015). Additionally, a recent study of the age of carbon in earlywood and latewood portions of annual oak rings during the mid-20th century bomb pulse indicated that the earlywood cellulose of oaks carried up to 50% of the atmospheric ^{14}C signal from the previous 1–2 years (Kromer et al., 2024). In conifers, carry-over from previous years was lower but extended into latewood in some species (Kromer et al., 2024). We note that in the Kromer et al. study, the authors took the novel step of removing rays from their oak samples. Rays cross ring boundaries and store carbon from previous years, suggesting that carry-over in other studies where rays were not removed could be larger. Other studies of oak during the bomb pulse also indicate some allocation of previous year(s) carbon to earlywood (Kudsk et al., 2018; Olsson & Possnert, 1992). Among the oak data used here, only one study (Fogtmann-Schulz et al., 2017) separated the EW and LW fractions in oak during a Miyake event. They observed that the LW portion recorded a rapid rise between 993 and 994 CE, but the EW portions were delayed by 1 year, that is, between 994 and 995 CE (Fogtmann-Schulz et al., 2017). These results and our observations support the idea that ^{14}C signals in ring-porous oaks could be delayed, with potential impacts on estimates of both event timing and modeled radiocarbon production. Additional studies of earlywood versus latewood formation in broadleaf species may improve estimates of the timing and ^{14}C production of past Miyake events.

Delayed signals in oak and variability in conifers from different sites were also observed in the less-well replicated 663 BCE Miyake event (Panyushkina et al., 2024). Comparing chronologies from a Japanese cedar, German oak, and two larch chronologies, one from Siberia and one from central Asia, Panyushkina et al. (2024) and others observed that the event was recorded over 2–3 years, though the records were not uniform. When modeled using *ticktack*, Panyushkina et al. (2024) observed that oak resulted in a delayed start, a more gradual rise in ^{14}C, and, unlike this study, a lower production rate relative to the conifer species, which maintained a more coherent response despite their latitudinal range of more than 30°. Even for the conifer species, however, the modeled start date, duration, and production of the event varied across sites, with high latitude Yamal larch documenting the most abrupt spike and the highest estimated production (4.5 times background). Several variables likely interact to generate this observed ^{14}C variability in conifer wood, including differences in latitude and altitude with their

effects on tropospheric ^{14}C concentration, tree phenology (uptake and allocation to wood), and the amount and age of stored NSCs used during wood formation.

5. Conclusion

In this study, we integrated new $\Delta^{14}C$ tree-ring data from Mongolia together with additional Northern Hemisphere $\Delta^{14}C$ tree-ring data sets to assess how tree functional traits influence Bayesian model estimates of radiocarbon production during Miyake events. We found little difference in the overall timing or pattern of measured $\Delta^{14}C$, or in modeled ^{14}C production in evergreen conifers and deciduous conifers growing under similar environmental conditions, likely due to their similar process of wood formation and carbon allocation strategies. We note however that the for the 993 CE event, with a lower signal to noise ratio in the ^{14}C data, parameter estimates were highly variable across groups. In a larger Northern Hemisphere data set, we observed general agreement in estimates of radiocarbon production across groups though deciduous broadleaf species produced less certain modeled estimates of start date, duration, and production. These differences highlight the role of species-specific carbon allocation strategies and storage dynamics as well as the effect of low signal to noise ratio in determining tree-ring records of radiocarbon during Miyake events. Similar to previous studies (Büntgen et al., 2018; Heaton et al., 2020), we observed that the 993 CE event, as recorded by trees, exhibited a different character from the 774 CE event, with more gradual changes in $\Delta^{14}C$ values and greater variability among sampled trees. Some of this variability may be attributable to the physiology of tree species, latitudinal variation in ^{14}C concentration, or seasonality of the event. Further research into these potential sources of variation across events is warranted. Future ^{14}C studies of past Miyake events and recent bomb-pulse studies using annually or sub annually dated tree rings should carefully consider the potential for uncertain signals in ring-porous species. Additional experiments designed to disentangle key sources of variation within the individual tree (e.g., physiology, phenology, stress), and from the production and circulation of ^{14}C, are required to improve our interpretation of annual and sub-annual measurements of ^{14}C from tree-rings in the context of past solar proton events.

Data Availability Statement

The tree-ring measurement data used to identify appropriate samples for AMS analysis in this study are archived at the WDS Paleo hosted by the NOAA National Centers for Environmental Information, and are published in Hessl et al. (2014, 2025a, 2025b), Hessl, Anchukaitis, et al. (2018), Hessl, Pederson, Byambasuren and Nachin (2018), Hessl, Pederson, Byambasuren, Nachin, and Leland (2018). AMS radiocarbon data generated by this study are provided in Supporting Information S1.

Acknowledgments
We thank everyone who participated in fieldwork, sample preparation, crossdating and chronology development. Support for this research was provided by the WVSGC NASA Graduate Research Fellowship Program, NSF P2C2 #1804121, NSF GRFP #2136524, NSF Solar Terrestrial #2411569, and NUM Grant #P2020-3988. Support for the NOSAMS radiocarbon lab measurements was provided by the WVSGC NASA Graduate Research Fellowship Program grant and NSF GRFP #1008434CR grant. NOSAMS acknowledges support from NSF by including the NSF Cooperative Agreement number, OCE-1755125.

References

Appenzeller, C., Holton, J. R., & Rosenlof, K. H. (1996). Seasonal variation of mass transport across the tropopause. *Journal of Geophysical Research*, *101*(D10), 15071–15078. https://doi.org/10.1029/96JD00821

Barbaroux, C., & Bréda, N. (2002). Contrasting distribution and seasonal dynamics of carbohydrate reserves in stem wood of adult ring-porous sessile oak and diffuse-porous beech trees. *Tree Physiology*, *22*(17), 1201–1210. https://doi.org/10.1093/treephys/22.17.1201

Bard, E., Miramont, C., Capano, M., Guibal, F., Marschal, C., Rostek, F., et al. (2023). A radiocarbon spike at 14 300 cal yr BP in subfossil trees provides the impulse response function of the global carbon cycle during the Late Glacial. *Philosophical Transactions. Series A, Mathematical, Physical, and Engineering Sciences*, *381*(2261), 20220206. https://doi.org/10.1098/rsta.2022.0206

Black, B. A., Pearl, J. K., Pearson, C. L., Pringle, P. T., Frank, D. C., Page, M. T., et al. (2023). A multifault earthquake threat for the Seattle metropolitan region revealed by mass tree mortality. *Science Advances*, *9*(39), eadh4973. https://doi.org/10.1126/sciadv.adh4973

Braziunas, T. F., Fung, I. Y., & Stuiver, M. (1995). The preindustrial atmospheric $^{14}CO_2$ latitudinal gradient as related to exchanges among atmospheric, oceanic, and terrestrial reservoirs. *Global Biogeochemical Cycles*, *9*(4), 565–584. https://doi.org/10.1029/95GB01725

Brehm, N., Bayliss, A., Christl, M., Synal, H.-A., Adolphi, F., Beer, J., et al. (2021). Eleven-year solar cycles over the last millennium revealed by radiocarbon in tree rings. *Nature Geoscience*, *14*(1), 10–15. https://doi.org/10.1038/s41561-020-00674-0

Brehm, N., Christl, M., Knowles, T. D. J., Casanova, E., Evershed, R. P., Adolphi, F., et al. (2022). Tree-rings reveal two strong solar proton events in 7176 and 5259 BCE. *Nature Communications*, *13*(1), 1. https://doi.org/10.1038/s41467-022-28804-9

Büntgen, U., Wacker, L., Galván, J. D., Arnold, S., Arseneault, D., Baillie, M., et al. (2018). Tree rings reveal globally coherent signature of cosmogenic radiocarbon events in 774 and 993 CE. *Nature Communications*, *9*(1), 3605. https://doi.org/10.1038/s41467-018-06036-0

Carbone, M. S., Ayers, T. J., Ebert, C. H., Munson, S. M., Schuur, E. A. G., & Richardson, A. D. (2023). Atmospheric radiocarbon for the period 1910–2021 recorded by annual plants. *Radiocarbon*, *65*(2), 357–374. https://doi.org/10.1017/RDC.2023.5

Carbone, M. S., Czimczik, C. I., Keenan, T. F., Murakami, P. F., Pederson, N., Schaberg, P. G., et al. (2013). Age, allocation and availability of nonstructural carbon in mature red maple trees. *New Phytologist*, *200*(4), 1145–1155. https://doi.org/10.1111/nph.12448

Chen, Y., Rademacher, T., Fonti, P., Eckes-Shephard, A. H., LeMoine, J. M., Fonti, M. V., et al. (2022). Inter-annual and inter-species tree growth explained by phenology of xylogenesis. *New Phytologist*, *235*(3), 939–952. https://doi.org/10.1111/nph.18195

Cliver, E. W., Schrijver, C. J., Shibata, K., & Usoskin, I. G. (2022). Extreme solar events. *Living Reviews in Solar Physics*, *19*(1), 2. https://doi.org/10.1007/s41116-022-00033-8

Dietze, M. C., Sala, A., Carbone, M. S., Czimczik, C. I., Mantooth, J. A., Richardson, A. D., & Vargas, R. (2014). Nonstructural carbon in woody plants. *Annual Review of Plant Biology*, *65*(1), 667–687. https://doi.org/10.1146/annurev-arplant-050213-040054

Epron, D., Bahn, M., Derrien, D., Lattanzi, F. A., Pumpanen, J., Gessler, A., et al. (2012). Pulse-labelling trees to study carbon allocation dynamics: A review of methods, current knowledge and future prospects. *Tree Physiology*, *32*(6), 776–798. https://doi.org/10.1093/treephys/tps057

Fogtmann-Schulz, A., Østbø, S. M., Nielsen, S. G. B., Olsen, J., Karoff, C., & Knudsen, M. F. (2017). Cosmic ray event in 994 C.E. recorded in radiocarbon from Danish oak. *Geophysical Research Letters*, *44*(16), 8621–8628. https://doi.org/10.1002/2017GL074208

Furze, M. E., Huggett, B. A., Aubrecht, D. M., Stolz, C. D., Carbone, M. S., & Richardson, A. D. (2019). Whole-tree nonstructural carbohydrate storage and seasonal dynamics in five temperate species. *New Phytologist*, *221*(3), 1466–1477. https://doi.org/10.1111/nph.15462

Gatz, D. F., & Smith, L. (1995). The standard error of a weighted mean concentration—I. Bootstrapping vs other methods. *Atmospheric Environment*, *29*(11), 1185–1193. https://doi.org/10.1016/1352-2310(94)00210-C

Golubenko, K., Usoskin, I., Rozanov, E., & Bard, E. (2025). New SOCOL:14C-Ex model reveals that the Late-Glacial radiocarbon spike in 12350 BC was caused by the record-strong extreme solar storm. *Earth and Planetary Science Letters*, *661*, 119383. https://doi.org/10.1016/j.epsl.2025.119383

Harrell, F. (2025). Harrelfe/Hmisc [R], (Original work published 2013). Retrieved from https://github.com/harrelfe/Hmisc

Heaton, T. J., Blaauw, M., Blackwell, P. G., Bronk Ramsey, C., Reimer, P. J., & Scott, E. M. (2020). The IntCal20 approach to radiocarbon calibration curve construction: A new methodology using Bayesian Splines and errors-in-variables. *Radiocarbon*, *62*(4), 821–863. https://doi.org/10.1017/RDC.2020.46

Heckert, N. A., & Filliben, J. J. (2003). *NIST handbook 148: DATAPLOT reference manual, Volume I: Commands* (Vol. 1). National Institute of Standards and Technology.

Hessl, A. E., Anchukaitis, K. J., Jelsema, C., Cook, B., Byambasuren, O., Leland, C., et al. (2018). Past and future drought in Mongolia. *Science Advances*, *4*(3), e1701832. https://doi.org/10.1126/sciadv.1701832

Hessl, A. E., Pederson, N., Anchukaitis, K. J., Burkhart, J., Byambasuren, O., Nachin, B., et al. (2014). NOAA/WDS Paleoclimatology—Hessl—Khorgo Lava pine—PISI—TRDB MONG039 [Dataset]. *NOAA National Centers for Environmental Information*. https://doi.org/10.25921/GPWE-4V32

Hessl, A. E., Pederson, N., Byambasuren, O., & Nachin, B. (2018). NOAA/WDS Paleoclimatology—Hessl—Uurgat Lava—Pisi—ITRDB MONG042 [Dataset]. *NOAA National Centers for Environmental Information*. https://doi.org/10.25921/B3AK-ET30

Hessl, A. E., Pederson, N., Byambasuren, O., Nachin, B., & Leland, C. (2018). NOAA/WDS Paleoclimatology—Hessl—Khorgo Lava Update—Pisi—ITRDB MONG041 [Dataset]. *NOAA National Centers for Environmental Information*. https://doi.org/10.25921/EGD3-4Q45

Hessl, A. E., Pederson, N., Nachin, B., Leland, C., Fernandez, J., de Graauw, K. K., & Zhu, J. (2025a). NOAA/WDS paleoclimatology—Hessl—Khorgo Lava larch—Lasi—ITRDB MNG044 [Dataset]. *NOAA National Centers for Environmental Information*. https://doi.org/10.25921/zjm0-6v92

Hessl, A. E., Pederson, N., Nachin, B., Leland, C., Fernandez, J., de Graauw, K. K., & Zhu, J. (2025b). NOAA/WDS Paleoclimatology—Hessl—Uurgat Lava Larch—Lasi—ITRDB MNG045 [Dataset]. *NOAA National Centers for Environmental Information*. https://doi.org/10.25921/xyyc-4m31

Hinckley, T., & Lassoie, J. (1981). Radial growth in conifers and deciduous trees: A comparison. *Mitteilungen der Forstlichen Bundesversuchsanstalt Wien*, *142*, 17–56.

Hua, Q., Barbetti, M., & Rakowski, A. Z. (2013). Atmospheric radiocarbon for the period 1950–2010. *Radiocarbon*, *55*(4), 2059–2072. https://doi.org/10.2458/azu_js_rc.v55i2.16177

Jull, A. J. T., Panyushkina, I. P., Lange, T. E., Kukarskih, V. V., Myglan, V. S., Clark, K. J., et al. (2014). Excursions in the ^{14}C record at A.D. 774–775 in tree rings from Russia and America. *Geophysical Research Letters*, *41*(8), 3004–3010. https://doi.org/10.1002/2014GL059874

Kagawa, A., Sugimoto, A., & Maximov, T. C. (2006). $^{13}CO_2$ pulse-labelling of photoassimilates reveals carbon allocation within and between tree rings. *Plant, Cell and Environment*, *29*(8), 1571–1584. https://doi.org/10.1111/j.1365-3040.2006.01533.x

Koldobskiy, S. A., Mekhaldi, F., Kovaltsov, G. A., & Usoskin, I. G. (2022). Multiproxy reconstructions of integral energy spectra for extreme solar particle events of 7176 BCE, 660 BCE, 775 CE and 994 CE. https://doi.org/10.1002/essoar.10512946.1

Kromer, B., Wacker, L., Friedrich, M., Lindauer, S., Friedrich, R., Bitterli, J., et al. (2024). Origin and age of carbon in the cellulose of mid-latitude tree rings. *Radiocarbon*, *66*(6), 1–16. https://doi.org/10.1017/RDC.2024.38

Kudsk, S. G. K., Olsen, J., Nielsen, L. N., Fogtmann-Schulz, A., Knudsen, M. F., & Karoff, C. (2018). What is the carbon origin of early-wood? *Radiocarbon*, *60*(5), 1457–1464. https://doi.org/10.1017/RDC.2018.97

Kuitems, M., Panin, A., Scifo, A., Arzhantseva, I., Kononov, Y., Doeve, P., et al. (2020). Radiocarbon-based approach capable of subannual precision resolves the origins of the site of Por-Bajin. *Proceedings of the National Academy of Sciences of the United States of America*, *117*(25), 14038–14041. https://doi.org/10.1073/pnas.1921301117

McDonald, L., Chivall, D., Miles, D., & Bronk Ramsey, C. (2019). Seasonal variations in the ^{14}C content of tree rings: Influences on radiocarbon calibration and single-year curve construction. *Radiocarbon*, *61*(1), 185–194. https://doi.org/10.1017/RDC.2018.64

Methods-NOSAMS. (2023). Nosams. Retrieved from https://www2.whoi.edu/site/nosams/

Mekhaldi, F., Adolphi, F., Herbst, K., & Muscheler, R. (2021). The signal of solar storms embedded in cosmogenic radionuclides: Detectability and uncertainties. *Journal of Geophysical Research: Space Physics*, *126*(8), e2021JA029351. https://doi.org/10.1029/2021JA029351

Mekhaldi, F., Muscheler, R., Adolphi, F., Aldahan, A., Beer, J., McConnell, J. R., et al. (2015). Multiradionuclide evidence for the solar origin of the cosmic-ray events of AD 774/5 and 993/4. *Nature Communications*, *6*(1), 8611. https://doi.org/10.1038/ncomms9611

Miyahara, H., Tokanai, F., Moriya, T., Takeyama, M., Sakurai, H., Ohyama, M., et al. (2022). Recurrent large-scale solar proton events before the onset of the Wolf grand solar minimum. *Geophysical Research Letters*, *49*(5), e2021GL097201. https://doi.org/10.1029/2021GL097201

Miyake, F., Hakozaki, M., Kimura, K., Tokanai, F., Nakamura, T., Takeyama, M., & Moriya, T. (2022). Regional differences in carbon-14 data of the 993 CE cosmic ray event. *Frontiers in Astronomy and Space Sciences*, *9*, 886140. https://doi.org/10.3389/fspas.2022.886140

Miyake, F., Masuda, K., & Nakamura, T. (2013). Another rapid event in the carbon-14 content of tree rings. *Nature Communications*, *4*(1), 1. https://doi.org/10.1038/ncomms2783

Miyake, F., Nagaya, K., Masuda, K., & Nakamura, T. (2012). A signature of cosmic-ray increase in ad 774–775 from tree rings in Japan. *Nature*, *486*(7402), 240–242. https://doi.org/10.1038/nature11123

Miyake, F., Panyushkina, I. P., Jull, A. J. T., Adolphi, F., Brehm, N., Helama, S., et al. (2021). A single-year cosmic ray event at 5410 BCE registered in ^{14}C of tree rings. *Geophysical Research Letters*, *48*(11), e2021GL093419. https://doi.org/10.1029/2021GL093419

Moser, L., Fonti, P., Büntgen, U., Esper, J., Luterbacher, J., Franzen, J., & Frank, D. (2010). Timing and duration of European larch growing season along altitudinal gradients in the Swiss Alps. *Tree Physiology*, *30*(2), 225–233. https://doi.org/10.1093/treephys/tpp108

Nakamura, T., Masuda, K., Miyake, F., Nagaya, K., & Yoshimitsu, T. (2013). Radiocarbon ages of annual rings from Japanese wood: Evident age offset based on IntCal09. *Radiocarbon*, *55*(2), 763–770. https://doi.org/10.1017/S0033822200057921

Němec, M., Wacker, L., Hajdas, I., & Gäggeler, H. (2010). Alternative methods for cellulose preparation for AMS measurement. *Radiocarbon*, *52*(3), 1358–1370. https://doi.org/10.1017/S0033822200046440

Olsson, I. U., & Possnert, G. (1992). ^{14}C activity in different sections and chemical fractions of Oak tree rings, AD 1938–1981. *Radiocarbon*, *34*(3), 757–767. https://doi.org/10.1017/S0033822200064055

Palacio, S., Maestro, M., & Montserratmarti, G. (2007). Seasonal dynamics of non-structural carbohydrates in two species of mediterranean sub-shrubs with different leaf phenology. *Environmental and Experimental Botany*, *59*(1), 34–42. https://doi.org/10.1016/j.envexpbot.2005.10.003

Panyushkina, I. P., Jull, A. J. T., Molnár, M., Varga, T., Kontul', I., Hantemirov, R., et al. (2024). The timing of the ca-660 BCE Miyake solar-proton event constrained to between 664 and 663 BCE. *Communications Earth & Environment*, *5*(1), 1–9. https://doi.org/10.1038/s43247-024-01618-x

Park, J., Southon, J., Fahrni, S., Creasman, P. P., & Mewaldt, R. (2017). Relationship between solar activity and Δ^{14}C peaks in AD 775, AD 994, and 660 BC. *Radiocarbon*, *59*(4), 1147–1156. https://doi.org/10.1017/RDC.2017.59

Pearl, J. K., Anchukaitis, K. J., Donnelly, J. P., Pearson, C., Pederson, N., Lardie Gaylord, M. C., et al. (2020). A late Holocene subfossil Atlantic white cedar tree-ring chronology from the northeastern United States. *Quaternary Science Reviews*, *228*, 106104. https://doi.org/10.1016/j.quascirev.2019.106104

Peltier, D. M. P., Carbone, M. S., McIntire, C. D., Robertson, N., Thompson, R. A., Malone, S., et al. (2023). Carbon starvation following a decade of experimental drought consumes old reserves in Pinus edulis. *New Phytologist*, *240*(1), 92–104. https://doi.org/10.1111/nph.19119

Rakowski, A. Z., Krąpiec, M., Huels, M., Pawlyta, J., & Boudin, M. (2018). Increase in radiocarbon concentration in tree rings from Kujawy Village (Se Poland) around ad 993–994. *Radiocarbon*, *60*(4), 1249–1258. https://doi.org/10.1017/RDC.2018.74

Rakowski, A. Z., Krąpiec, M., Huels, M., Pawlyta, J., Dreves, A., & Meadows, J. (2015). Increase of radiocarbon concentration in tree rings from Kujawy (SE Poland) around AD 774-775. *Nuclear Instruments and Methods in Physics Research B*, *361*, 564–568. https://doi.org/10.1016/j.nimb.2015.03.035

Rakowski, A. Z., Krąpiec, M., Huels, M., Pawlyta, J., & Wiktorowski, D. (2022). The Miyake event in 993 CE recorded in Oak sub-annual tree rings from Kujawy (Poland). *Radiocarbon*, *64*(6), 1597–1606. https://doi.org/10.1017/RDC.2022.54

Reimer, P. J., Austin, W. E. N., Bard, E., Bayliss, A., Blackwell, P. G., Bronk Ramsey, C., et al. (2020). The IntCal20 northern Hemisphere radiocarbon age calibration curve (0–55 cal kBP). *Radiocarbon*, *62*(4), 725–757. https://doi.org/10.1017/RDC.2020.41

Richardson, A. D., Carbone, M. S., Huggett, B. A., Furze, M. E., Czimczik, C. I., Walker, J. C., et al. (2015). Distribution and mixing of old and new nonstructural carbon in two temperate trees. *New Phytologist*, *206*(2), 590–597. https://doi.org/10.1111/nph.13273

Richardson, A. D., Carbone, M. S., Keenan, T. F., Czimczik, C. I., Hollinger, D. Y., Murakami, P., et al. (2013). Seasonal dynamics and age of stemwood nonstructural carbohydrates in temperate forest trees. *New Phytologist*, *197*(3), 850–861. https://doi.org/10.1111/nph.12042

Rodgers, K. B., Mikaloff-Fletcher, S. E., Bianchi, D., Beaulieu, C., Galbraith, E. D., Gnanadesikan, A., et al. (2011). Interhemispheric gradient of atmospheric radiocarbon reveals natural variability of Southern Ocean winds. *Climate of the Past*, *7*(4), 1123–1138. https://doi.org/10.5194/cp-7-1123-2011

Rossi, S., Rathgeber, C. B. K., & Deslauriers, A. (2009). Comparing needle and shoot phenology with xylem development on three conifer species in Italy. *Annals of Forest Science*, *66*(2), 2. https://doi.org/10.1051/forest/2008088

Sakurai, H., Tokanai, F., Miyake, F., Horiuchi, K., Masuda, K., Miyahara, H., et al. (2020). Prolonged production of ^{14}C during the ~660 BCE solar proton event from Japanese tree rings. *Scientific Reports*, *10*(1), 1. https://doi.org/10.1038/s41598-019-57273-2

Schoettle, A. W., Fahey, T. J., & Shoettle, A. W. (1994). Foliage and fine root longevity of pines. *Ecological Bulletins*, *43*, 136–153.

Schuur, E. A. G., & Trumbore, S. E. (2006). Partitioning sources of soil respiration in boreal black spruce forest using radiocarbon. *Global Change Biology*, *12*(2), 165–176. https://doi.org/10.1111/j.1365-2486.2005.01066.x

Scifo, A., Abi Nassif, T., Conti, M., Bayliss, A., Doeve, P., & Dee, M. W. (2024). New data fails to replicate the small-scale radiocarbon anomalies in the early second millennium CE. *Radiocarbon*, *66*(3), 1–14. https://doi.org/10.1017/RDC.2024.52

Scifo, A., Kuitems, M., Neocleous, A., Pope, B. J. S., Miles, D., Jansma, E., et al. (2019). Radiocarbon production events and their potential relationship with the Schwabe cycle. *Scientific Reports*, *9*(1), 17056. https://doi.org/10.1038/s41598-019-53296-x

Scott, E. M., Naysmith, P., & Dunbar, E. (2023). Preliminary results from glasgow International radiocarbon Intercomparison. *Radiocarbon*, *66*(5), 1–8. https://doi.org/10.1017/RDC.2023.64

Sharma, U., Zhang, Q., Dennis, J., & Pope, B. J. S. (2023). ticktack: A Python package for carbon box modelling. *Journal of Open Source Software*, *8*(83), 5084. https://doi.org/10.21105/joss.05084

Southon, J. R., & Magana, A. L. (2010). A comparison of cellulose extraction and ABA pretreatment methods for AMS ^{14}C dating of ancient wood. *Radiocarbon*, *52*(3), 1371–1379. https://doi.org/10.1017/S0033822200046452

Stuiver, M., & Polach, H. A. (1977). Discussion reporting of ^{14}C data. *Radiocarbon*, *19*(3), 355–363. https://doi.org/10.1017/S0033822200003672

Usoskin, I. G., Koldobskiy, S. A., Kovaltsov, G. A., Rozanov, E. V., Sukhodolov, T. V., Mishev, A. L., & Mironova, I. A. (2020). Revisited reference solar proton event of 23 February 1956: Assessment of the cosmogenic-Isotope method sensitivity to extreme solar events. *Journal of Geophysical Research: Space Physics*, *125*(6), e2020JA027921. https://doi.org/10.1029/2020JA027921

Usoskin, I. G., Kromer, B., Ludlow, F., Beer, J., Friedrich, M., Kovaltsov, G. A., et al. (2013). The AD775 cosmic event revisited: The Sun is to blame. *Astronomy & Astrophysics*, *552*, L3. https://doi.org/10.1051/0004-6361/201321080

Uusitalo, J., Arppe, L., Hackman, T., Helama, S., Kovaltsov, G., Mielikäinen, K., et al. (2018). Solar superstorm of AD 774 recorded subannually by Arctic tree rings. *Nature Communications*, *9*(1), 1. https://doi.org/10.1038/s41467-018-05883-1

Uusitalo, J., Golubenko, K., Arppe, L., Brehm, N., Hackman, T., Hayakawa, H., et al. (2024). Transient offset in ^{14}C after the Carrington event recorded by polar tree rings. *Geophysical Research Letters*, *51*(5), e2023GL106632. https://doi.org/10.1029/2023GL106632

Von Felten, S., Hättenschwiler, S., Saurer, M., & Siegwolf, R. (2007). Carbon allocation in shoots of alpine treeline conifers in a CO_2 enriched environment. *Trees*, *21*(3), 283. https://doi.org/10.1007/s00468-006-0118-7

Zhang, Q., Sharma, U., Dennis, J. A., Scifo, A., Kuitems, M., Büntgen, U., et al. (2022). Modelling cosmic radiation events in the tree-ring radiocarbon record. *Proceedings of the Royal Society A: Mathematical, Physical and Engineering Sciences*, *478*(2266), 20220497. https://doi.org/10.1098/rspa.2022.0497